University of Baghdad
College of Engineering
JE
JOURNAL OF ENGINEERING

Journal of Engineering

journal homepage: www.jcoeng.edu.iq

Volume 32 Number 9 September 2026

Nonlinear Finite Element Analysis of Steel Fiber Reinforced Concrete Beams Subjected to Pure Torsion

Hayder A. Al-Baghdadi [1], **Iman Munadhil Abbas Al-Damad** [1,*], **Ehab G. Al-Hasany** [2], **Mustafa Qasim Dows** [3]

[1] Department of Civil Engineering, College of Engineering, University of Baghdad, Baghdad, Iraq
[2] World Bank Financed Projects, Ministry of Education, Baghdad, Iraq
[3] Department of Mechanical Engineering, College of Engineering, University of Baghdad, Baghdad, Iraq

ABSTRACT

Steel fiber reinforced concrete (SFRC) can enhance post-cracking tensile resistance through fiber bridging across cracks; however, the torsional contribution of fibers is still not explicitly addressed in most design provisions. This study develops a three-dimensional nonlinear finite element (FE) model in ABAQUS to evaluate the response of SFRC beams subjected to pure torsion. The concrete response was simulated using the Concrete Damage Plasticity (CDP) model, while the tensile softening behavior of SFRC was represented using stress–crack opening displacement relationships derived from experimental material characterization data. The FE model was validated against two independent experimental programs reported in the literature, covering beams with different fiber contents and transverse reinforcement ratios. The validation was performed through comparisons of torque–twist response, ultimate torsional capacity, and crack patterns. Following validation, a parametric study was conducted to examine the effects of SFRC post-cracking tensile softening behavior, concrete compressive strength, stirrup bar diameter, and stirrup spacing. The results showed that SFRC tensile softening behavior significantly influenced residual torsional resistance, deformation capacity, and post-cracking response. Increasing concrete compressive strength improved both cracking torque and ultimate torsional capacity, although the improvement was not directly proportional to the strength increase. Reducing stirrup spacing was more effective than increasing stirrup bar diameter because closer stirrups improved crack control and enhanced the torsion-resisting mechanism. The findings confirm that steel fibers and transverse reinforcement provide complementary contributions to torsional resistance under pure torsion.

Keywords: Finite element analysis, Torque–twist response, Steel fiber reinforced concrete, Pure torsion, Post-cracking behavior.

*Corresponding author
Peer review under the responsibility of University of Baghdad.
https://doi.org/10.31026/j.eng.2026.09.07

Article received: 26/06/2026
Article revised: 29/07/2026
Article accepted: 09/08/2026
Article published: 01/09/2026

1. INTRODUCTION

Torsional moments occur in many reinforced concrete structures because of geometric irregularities, curved layouts, eccentric loading conditions, and load-transfer mechanisms. In practice, torsion seldom acts alone and may act concurrently with bending moments and shear forces, and sometimes also with axial loads. The behavior of reinforced concrete (RC) members is mostly nonlinear, with a marked loss in stiffness as soon as torsional cracking occurs. These reductions are typically more significant than those associated with flexural cracking and must therefore be predicted accurately, as they strongly influence the torsional response of structural members **(Macgregor and Wight, 2005)**.

It is well established that using steel fibers in concrete is an effective way of improving the tensile behavior of concrete by bridging stresses across cracks. Steel fibers have been thoroughly investigated, both experimentally and analytically, for their effectiveness in improving cracking resistance, ductility, energy absorption capacity, and post-cracking performance at both the material and structural levels **(Pfyl, 2003; Lövgren, 2005; Minelli, 2005; Amin, 2015; Facconi et al., 2021a; Facconi et al., 2021b; Al-Damad et al., 2025)**. Consequently, SFRC has gained steady acceptance in both the research and engineering communities, which has driven the development of design provisions for flexure and shear in several international codes and guidelines, including **(*fib* Model Code 2010, 2013; DAfStb Guideline, 2015; AS3600, 2018; ACI 318, 2019)**.

However, the torsional design of SFRC members remains insufficiently addressed in current design provisions. Current code-based methods mainly adopt traditional space-truss models, in which torsional resistance is attributed to fully closed stirrups and longitudinal reinforcement. Although these methods generally guarantee safe designs, they typically do not explicitly account for the contribution of steel fibers to crack control and post-cracking load transfer. As a result, the advantages of fibers are only partially realized, often leading to conservative designs and excessive amounts of manually placed transverse reinforcement **(Okay and Engin, 2012; Faccin et al., 2021; Oettel, 2023; Facconi et al., 2025)**.

Previous experimental investigations have consistently shown that steel fibers can significantly enhance the torsional performance of RC members by increasing cracking torque, improving post-cracking stiffness, delaying crack propagation, and enhancing ductility **(Foster and Voo, 2004; Foster et al., 2006; Amin and Bentz, 2018; Al-Damad and Foster, 2022; Rakaa and Abbas, 2024; Al-Damad et al., 2025)**. However, experimental testing alone cannot easily isolate the influence of individual parameters governing torsional behavior, particularly those associated with the post-cracking constitutive response of SFRC, compressive strength of concrete, and the ratio of transverse rebar. Furthermore, the interaction between these parameters and their influence on the development of torsional resistance mechanisms remain inadequately understood.

As structural design transitions toward performance-based processes, there is a demand for efficient numerical means to accurately capture the entire torsional response of SFRC members, including stiffness degradation, and post-cracking behavior. This makes reliable numerical models an efficient instrument for parametric studies that would otherwise necessitate lengthy and costly experimental campaigns. This is especially crucial for torsion-dominated members, as local fracture mechanisms can control the global structural response **(Lim et al., 1987; Mansur et al., 1989; El-Niema, 1993; Rao and Seshu, 2005; Minelli and Vecchio, 2006; Chalioris and Karayannis, 2009; Lee et al., 2012; Ju et al., 2015; Amin and Bentz, 2018)**.

Pure torsion was considered in this study because it provides a controlled loading condition for isolating the torsion-resisting mechanism without the additional interaction of flexure and shear. Although structural members in practice are often subjected to combined actions, pure torsion tests are essential for understanding the fundamental contribution of concrete, steel fibers, longitudinal reinforcement, and stirrups to torsional resistance. This loading condition also allows a clearer evaluation of the torque–twist response, post-cracking stiffness degradation, and residual torsional resistance of SFRC members. Therefore, pure torsion was adopted as a suitable basis for validating the numerical model and for conducting the subsequent parametric investigation.

To address these knowledge gaps, the current study develops a three-dimensional nonlinear finite element model using ABAQUS **(Dassault Systèmes, 2019)** to investigate the torsional response of SFRC beams subjected to pure torsion. The model is validated with experimental data from previous studies before being used to explore the influence of selected material and reinforcement parameters on torsional response.

2. RESEARCH SIGNIFICANCE

While earlier experimental studies have established the positive contribution of steel fibers in resisting torsion to reinforced concrete members, there is still inadequate quantification of how fiber bridging action, concrete compressive strength and transverse reinforcement individually influence this aspect. This limits the efficient use of SFRC in members where torsion is a governing design action.

The significance of this study lies in developing a validated nonlinear FE model capable of representing the torque–twist response, ultimate torsional capacity, and main damage characteristics of SFRC beams subjected to pure torsion. The model is then used to evaluate the influence of key parameters, including post-cracking tensile softening behavior, concrete compressive strength, stirrup diameter, and stirrup spacing.

The study provides insight into the complementary roles of steel fibers and conventional transverse reinforcement in torsion resistance. The findings may support the development of more rational numerical modeling approaches and future design recommendations for SFRC members subjected to torsion.

3. NUMERICAL MODELING

The torsional behavior of SFRC beams under pure torsion was studied using three-dimensional nonlinear FEMs in ABAQUS **(Dassault Systèmes, 2019)**. The numerical models were developed to reproduce the experimental specimens tested by **(Facconi et al., 2021a; Al-Damad et al., 2025)**, including the beam geometry, reinforcement layout, material properties, support conditions, and loading arrangement. A modeling strategy was chosen that could accurately represent the nonlinear torque–twist response of the beams throughout the entire loading path, including stiffness degradation and post-cracking behavior. Details of the FE discretization, reinforcement modeling, boundary conditions, and loading procedure are presented in the following subsections, while the adopted constitutive material models are described in next section.

3.1 Numerical Work Program

The numerical work program was organized into two main stages: model validation and parametric investigation. In the first stage, FEMs were developed to reproduce the experimental members tested by **(Facconi et al., 2021a; Al-Damad et al., 2025)**. The validation stage included comparisons between the numerical and experimental results in terms of torque–twist response, ultimate torsional capacity, and crack patterns. This stage was used to assess the ability of the adopted modeling approach and constitutive material models to reproduce the torsional response of RC and SFRC beams subjected to pure torsion. In the second stage, the validated numerical model was used to conduct a parametric study to investigate the influence of selected material and reinforcement parameters on the torsional response of SFRC beams. The parameters investigated included the post-cracking tensile softening behavior of SFRC, concrete compressive strength, stirrup bar diameter, and stirrup spacing. During each parametric investigation, the remaining parameters were kept constant as much as possible to isolate the effect of the parameter under consideration. The numerical results were evaluated mainly in terms of torque–twist response, torsional stiffness, ultimate torsional capacity, residual torsional resistance, and post-cracking behavior. A summary of the numerical work program, including the validation stage and the main parametric investigations, is presented in **Table 1**.

Table 1. Summary of the numerical work program.

Stage	Purpose	Main variables	Main outputs
Model validation	To validate the FEM against experimental results	Beam geometry, fiber content, and transverse reinforcement ratio based on tested specimens	Torque–twist response, ultimate torsional capacity, and crack patterns
SFRC tensile softening study	To evaluate the effect of post-cracking tensile behavior	Different stress–COD relationships	Residual torsional resistance and post-cracking response
Concrete strength study	To evaluate the effect of concrete compressive strength	35, 60, 80, and 100 MPa	Cracking torque, ultimate torsional capacity, and stiffness
Stirrup diameter study	To evaluate the effect of transverse reinforcement area	8, 10, and 12 mm stirrup diameters	Torsional capacity and deformation response
Stirrup spacing study	To evaluate the effect of transverse reinforcement distribution	100, 200, 300, and 400 mm stirrup spacing	Torsional capacity, stiffness, and post-cracking response

3.2 Finite Element Modeling

The geometry and rebar details of the experimental specimens were reproduced in ABAQUS. A typical FEM, including the reinforcement layout, is shown on **Fig. 1**. The concrete beams were modeled as three-dimensional deformable solid bodies using eight-node linear brick elements with reduced integration and hourglass control (C3D8R). All concrete components were assigned homogeneous solid sections.
The longitudinal reinforcement and transverse stirrups were modeled discretely using two-node three-dimensional truss elements (T3D2). The reinforcement was embedded within the concrete using the embedded region constraint available in ABAQUS, thereby enforcing displacement compatibility between the steel reinforcement and the surrounding concrete.

This approach assumes a full bond between the reinforcement and concrete throughout the analysis. Although this assumption is commonly adopted in nonlinear FE modeling of reinforced concrete members, it does not explicitly account for possible bond-slip effects.
A structured mesh comprising predominantly hexahedral elements was adopted for all models. To ensure an appropriate balance between computational efficiency and solution accuracy, a mesh sensitivity study was performed using different concrete element sizes. Based on the outcomes of this study, an element size of 30 mm was selected for the concrete mesh, as further mesh refinement resulted in only minor changes in the predicted torque–twist response while increasing the computational cost. To quantify the mesh sensitivity, additional analyses were carried out using representative concrete element sizes of 20 mm, 30 mm, and 40 mm. The variation in the predicted ultimate torque was minor. Therefore, the 30 mm mesh was adopted as it provided a suitable balance between numerical accuracy and computational efficiency. The same mesh size was used consistently in the validation and parametric models to ensure comparable results.

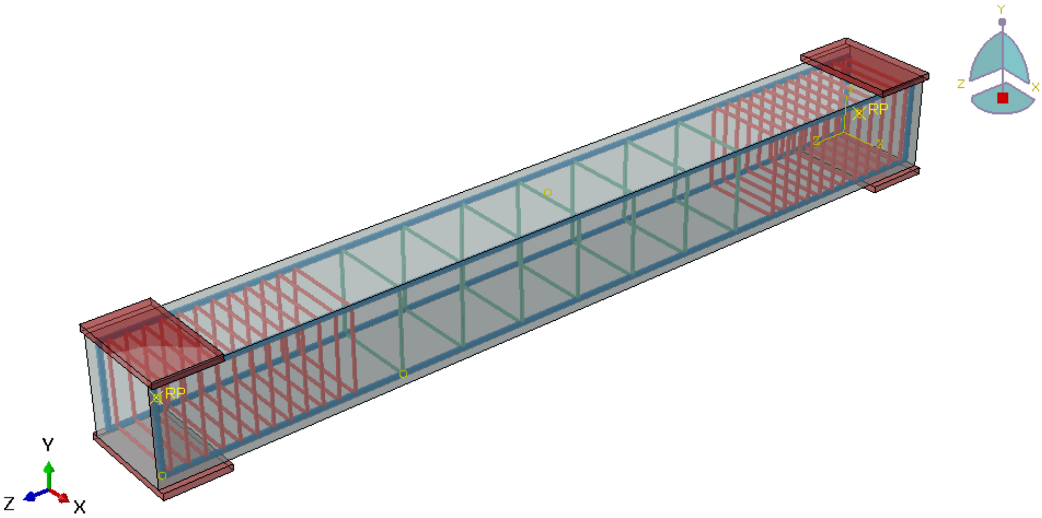

Figure 1. Three-dimensional FE model and reinforcement layout.

3.3 Specimen Geometry and Experimental Details

The finite element models were developed to reproduce the geometry, reinforcement details, material properties, and loading arrangements of the experimental specimens reported by **(Al-Damad et al., 2025; Facconi et al., 2021a)**. The validation specimens included RC and SFRC beams with different fiber dosages and transverse reinforcement configurations. The main parameters considered in the modeling included the beam dimensions, longitudinal reinforcement, stirrup diameter and spacing, concrete compressive strength, and fiber volume or dosage.
For the specimens reported by **(Al-Damad et al., 2025)**, the beams had a rectangular cross-section of 250 mm × 450 mm and an overall length of 6300 mm. The longitudinal reinforcement consisted of 16 mm diameter deformed bars, while 10 mm diameter stirrups were used where transverse reinforcement was provided. The investigated fiber dosages were 0, 30, and 60 kg/m^3, and the concrete compressive strengths were assigned according to the experimental material characterization results.
For the specimens reported by **(Facconi et al., 2021a)**, the beams had a square cross-section of 300 mm × 300 mm and a length of 2700 mm. The specimens included different

longitudinal reinforcement diameters, stirrup spacings, and steel fiber dosages. The material properties and reinforcement details used in the FE models were assigned according to the corresponding experimental data.

In both experimental programs, pure torsion was applied through loading arrangements that generated a twisting moment along the test region of the beam. The FE models reproduced the experimental boundary and loading conditions as closely as possible by using reference points and kinematic coupling at the beam ends.

3.4 Boundary Conditions and Loading

The boundary conditions and loading procedure adopted in the FE model were selected to reproduce the experimental pure torsion setup. The boundary conditions were applied through two reference regions located at the beam ends. The translational degrees of freedom were restrained as required to prevent rigid-body motion, while rotations about the longitudinal axis were controlled to reproduce the torsional loading condition. Two opposite rotations were applied at the beam ends, generating two opposite torques and producing a nearly uniform torsional moment along the test region. Using a ramp amplitude, the rotations were ramped in increments until the target level of twist was achieved.

The finite element analysis was performed with the same boundary conditions and loading arrangement used in the experiments to capture the pure torsional loading. At each end of the beam, reference points were established and connected to the respective support rings via kinematic constraints, ensuring that forces and moments were uniformly transferred between the reference points and the beam ends.

Because of the pure torsion simulation framework, all translational and rotational DOF were constrained at the reference points of degrees 1 and 2, except for the rotation of the beam's longitudinal axis. This setup allowed for torsional loading of the beam without any rigid-body motion.

A rotation-controlled loading scheme was employed to preserve numerical stability and capture the complete torque–twist response, including the post-cracking region. The reaction moments about the longitudinal axis were recorded at each increment of rotation and used to determine the applied torque.

4. MATERIAL MODELS

Accurate representation of material behavior is essential for predicting the nonlinear torsional response of SFRC beams. In this study, constitutive models were assigned to the reinforcing steel, conventional concrete, and SFRC to represent the main mechanisms governing the torque–twist response, including yielding of reinforcement, concrete compressive nonlinearity, tensile cracking, stiffness degradation, and post-cracking tensile resistance provided by steel fibers. The material models adopted in the FE analyses are described in the following subsections.

4.1 Stress-Strain Model of Reinforcing Steel

The rebar was modeled using an elastic–plastic constitutive relationship. The stress–strain response was assumed to be linear elastic up to the yield stress, followed by a strain-hardening branch until the ultimate tensile strength was reached. The steel properties were defined based on the material properties reported in the corresponding experimental studies used for model validation.

For the specimens reported by **(Al-Damad et al., 2025)**, the reinforcement cages were prepared using nominally 500 MPa deformed rebars. The specimens contained 16 mm diameter longitudinal deformed rebars, while 10 mm diameter bars were used as transverse reinforcement where stirrups were provided. The average measured yield strengths of the 10 mm and 16 mm bars were 582 MPa and 579 MPa, respectively, while the corresponding measured elastic moduli were 203 and 194 GPa. The ultimate tensile strength values were assigned according to the experimental material data reported by **(Al-Damad et al., 2025)**. These values were adopted in the FE models to define the elastic modulus, yielding behavior, and strain-hardening response of the transverse stirrups and longitudinal reinforcement.

For the specimens reported by **(Facconi et al., 2021a)**, the steel properties were assigned according to the measured properties of the deformed rebars used in each test series. The modeled specimens included 18 mm longitudinal reinforcement and 6 mm stirrups for the beams with transverse reinforcement, while the beam without stirrups included 18 mm longitudinal reinforcement only. The reported steel parameters include the nominal bar diameter, mean yield strength, ultimate tensile strength, and strain at ultimate strength. The relevant yield strengths ranged from 485 MPa to 567 MPa, while the corresponding ultimate tensile strengths ranged from 597 MPa to 670 MPa, depending on the bar diameter and test series. Where the elastic modulus was not explicitly reported, a value of 200 GPa was adopted for the reinforcing steel.

The same constitutive approach was used for both longitudinal rebar and transverse stirrups. The reinforcement was modeled as embedded truss elements; therefore, only axial stresses and strains were considered in the reinforcing bars.

4.2 Stress-Strain Model of Concrete (Compressive and Tensile)

The nonlinear behavior of concrete was simulated using the Concrete Damage Plasticity Model (CDPM) available in ABAQUS **(Dassault Systèmes, 2019)**. The CDPM is based on isotropic damaged elasticity combined with plasticity and can represent concrete cracking, crushing, and stiffness degradation under both compressive and tensile loading conditions **(Lubliner et al., 1989; Lee and Fenves, 1998)**. The implementation of the CDPM requires the definition of elastic properties, plasticity parameters, and uniaxial tensile and compressive stress–strain relationships **(Chen et al., 2007; Reuter et al., 2018)**. The adopted elastic and plastic parameters for the CDPM are summarized in **Table 2**.

For the implementation of the CDPM, the compressive stress–strain relationship was expressed as compressive stress versus inelastic strain, while the tensile response was formulated in terms of tensile stress versus cracking strain. Tensile and compressive damage variables, which represent stiffness degradation after cracking and crushing damage, respectively. These damage variables were assigned consistently with the adopted tensile and compressive constitutive relationships. The nonlinear analyses were performed using displacement-controlled loading with automatic incrementation. Convergence was monitored using the standard ABAQUS force and displacement residual criteria, and smaller increments were used near the cracking and post-cracking stages to improve numerical stability.

For the elastic response, concrete was defined by its elastic modulus (E_c) and Poisson's ratio (ν). The elastic modulus was calculated according to the **(ACI 318, 2019)** provisions. The uniaxial compressive stress–strain relationship was defined using the model proposed by **(Saenz, 1964)**, whereas the tensile response was represented using the tension-softening model developed by **(Hordijk, 1992)**. These constitutive relationships were incorporated into the CDPM to simulate the nonlinear response of concrete throughout the analysis.

Table 2. Elastic and plastic parameters adopted for the CDPM in ABAQUS.

E_c (MPa)	ν	ξ	K_c	f_{bo}/f_{co}	μ	Ψ
30900	0.2	0.1	0.667	1.16	0.001	45

The same CDPM framework was adopted for both normal-strength concrete (NC) and high-strength concrete (HSC) cases considered in parametric study. For the HSC cases with compressive strengths of 80 MPa and 100 MPa, the concrete elastic modulus and the uniaxial compressive and tensile stress–strain relationships were updated according to the corresponding compressive strength. The CDPM plasticity parameters listed in **Table 2** were kept unchanged for all concrete strength levels. Therefore, the HSC cases were not modeled using a different constitutive framework; rather, they were represented by strength-dependent material input data within the same CDPM formulation.

4.3 Tensile Stress-Strain Model of SFRC

Unlike conventional concrete, SFRC retains a residual tensile resistance after cracking through the crack-bridging action of the fibers. This residual capacity is particularly significant in members subjected to torsion, where the overall response depends strongly on the capability of the cracked section to continue transferring tensile stress across inclined torsional cracks.

In the present study, the tensile behavior of SFRC was represented using post-cracking softening relationships derived from the residual tensile strengths measured in the corresponding experimental material characterization tests. These relationships define the residual stress transferred across cracks once the tensile strength of the concrete matrix is exceeded. This approach enabled the contribution of fiber bridging to stiffness degradation, residual torsional resistance, and post-cracking behavior to be captured in the FE simulations.

It is very important to note that the tensile softening response of SFRC is not a single deterministic material curve, even for specimens with the same nominal fiber dosage and concrete mixture. The post-cracking response depends on the actual number of fibers crossing the crack plane, together with their orientation, distribution, embedment length, and local bond conditions. Consequently, different stress–crack opening displacement (stress–COD) curves may be obtained for specimens belonging to the same nominal material group. This scatter reflects the inherent randomness of SFRC at the cracked section and should not be interpreted as inconsistency in the experimental data. In the work of **(Al-Damad et al., 2025)**, fiber contribution was related to crack width and fiber engagement, and the factor K_s was introduced to account for the bias in fiber orientation caused by casting and for the randomness of fiber distribution in the hardened concrete. Likewise, **(Facconi et al., 2021a)** reported appreciable scatter in the residual tensile properties obtained from three-point bending tests, as reflected in the reported coefficients of variation for the residual strengths.

For this reason, more than one CDP tensile softening definition was adopted in parametric analysis. As presented in **Fig. 2**, different tensile stress–COD relationships were assigned to capture the experimentally observed variation in residual tensile resistance among the SFRC specimens. Although several beams shared the same nominal fiber dosage, their softening curves differed because the effective fiber bridging at the crack plane is governed by the local fiber distribution and orientation rather than by the nominal dosage alone. This approach allowed the numerical study to assess how realistic variations in post-cracking tensile behavior influence the torque–twist response, stiffness degradation, residual torsional capacity, and post-cracking behavior of SFRC beams.

The tensile stress–COD relationships used in the validation models were defined separately for each experimental program. The curves shown in **Fig. 2** correspond to the specimens reported by **(Al-Damad et al., 2025)**, while the corresponding softening relationships for the specimens of **(Facconi et al., 2021a)** were likewise incorporated in the FEMs. The legend in **Fig. 2** follows the specimen nomenclature adopted in **(Al-Damad et al., 2025)**.

For the validation models, the softening relationships were assigned according to the fiber dosage and material properties reported in the experimental studies. Where multiple stress–COD curves were available for specimens of the same nominal material, the curve corresponding to the tested specimen was used when available; otherwise, an average or representative softening response was adopted. In the parametric investigation, the stress–COD relationships were used and are discussed further in Section 6.1.

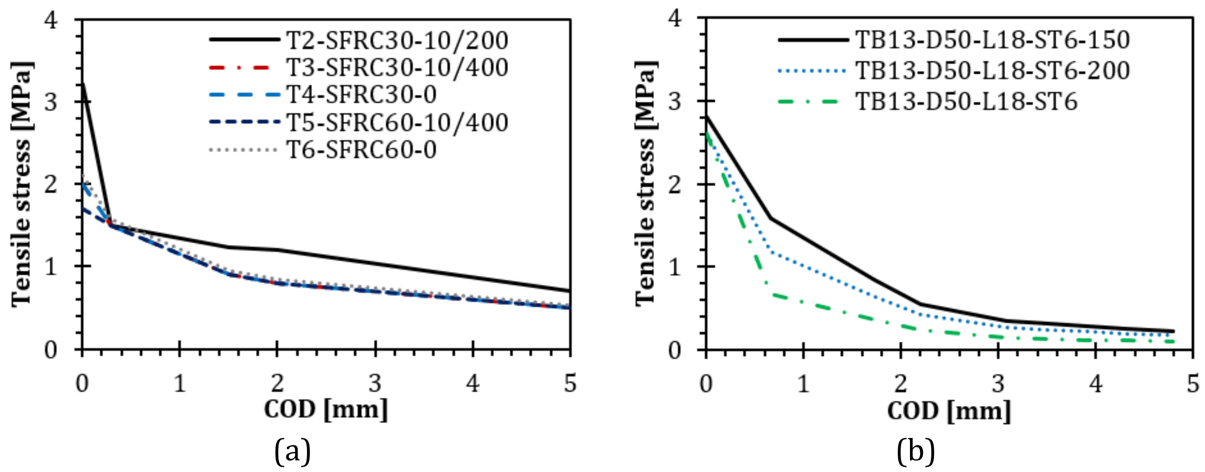

Figure 2. Tensile stress–COD relationships adopted for the SFRC specimens: (a) **(Al-Damad et al., 2025)**; (b) **(Facconi et al., 2021a)**.

5. MODEL VALIDATION

Prior to undertaking the parametric study, the developed FEM was validated against independent experimental investigations conducted by **(Al-Damad et al., 2025)** and **(Facconi et al., 2021a)**. The validation process was performed at both the global and local levels. At the global level, the predicted torque–twist responses and ultimate torsional capacities were compared with the experimental measurements. At the local level, the crack patterns and failure mechanisms obtained from the numerical analyses were evaluated against the observed experimental behavior. The results presented in the following subsections demonstrate the ability of the model to accurately reproduce the experimentally observed behavior for a range of fiber contents and transverse reinforcement ratios and give confidence in its suitability for conducting the subsequent parametric studies.

5.1 Torque-Twist Curves

5.1.1 Comparing with the Test Outcomes of Case Study Number I

The validity of the developed FEM was assessed by comparing the predicted torque–twist responses with the test results reported by **(Al-Damad et al., 2025)**, as shown in **Fig. 3**. The comparison includes both conventional RC and SFRC beams with varying fiber contents and transverse reinforcement ratios.

The torque–twist response was used as the main global indicator for evaluating torsional performance. In this response, the initial slope represents the uncracked torsional stiffness, while the change in slope after cracking reflects stiffness degradation and redistribution of stresses across concrete, steel fibers, and transverse reinforcement. The twist corresponding to peak torque indicates deformation capacity, whereas the descending or residual branch reflects the ability of the cracked member to maintain torsional resistance after damage localization. Therefore, the torque–twist curves were used not only to compare ultimate torsional capacity but also to evaluate stiffness degradation, deformation capacity, and post-cracking torsional resistance.

Overall, the developed model reproduces the global torsional behavior with good accuracy for most of the investigated beams. The model was satisfactory in predicting first crack load, post-cracking stiffness and failure load. In addition, the numerical model accurately captures the transition from the uncracked to the cracked state and reproduces the subsequent nonlinear response up to failure. Furthermore, the influence of both steel fibers and stirrups on torsional performance is consistently reflected in the numerical predictions.

For specimens T1-PC-10/200, T2-SFRC30-10/200, T3-SFRC30-10/400, and T5-SFRC60-10/400 (**Figs. 3a, 3b, 3c, and 3e**), the FEM closely reproduces the experimentally observed ascending branch and peak torsional capacity. Although the numerical responses are generally smoother than the experimental curves, the overall stiffness and strength characteristics are captured with high accuracy. The smoother numerical response is attributed to the crack behavior formulation adopted in the CDPM, whereas the experimental curves reflect local cracking events and stress redistributions associated with progressive cracking and local damage accumulation.

The experimental response in specimen T2-SFRC30-10/200 (**Fig. 3b**) shows a remarkable sudden drop in stiffness after the peak torque, whereas the numerical model predicts a more progressive reduction. The numerically smoother response is due to the non-local mechanism available with the CDPM, which describes cracking with smeared tensile damage and plastic strain localization instead of discrete crack surfaces, while the experiment is controlled by localized crack growth and sudden stress redistribution.

For specimens T4-SFRC30-0 and T6-SFRC60-0 (**Figs. 3d and 3f**), which contain no transverse reinforcement, the FEM predicts the peak torque accurately, although the reduction in the torque carried after the peak is less abrupt relative to the experimental findings. The torsional capacity in the tests was lost at higher post-peak loads due to localized crack propagation and failure mechanisms. In contrast, the numerical model spreads the damage over a set area, which in turn causes a gradual torque drop. However, the global response and failure load is reasonably captured.

Table 3 compares the experimentally measured ultimate torsional capacities with the numerical predictions. Good agreement is found for all specimens, with the ratio ($T_{u,test}/T_{u,FEM}$) in the range of 0.99 to 1.01. The mean value of the ratio is 1.00, which indicates that the FEM provides an essentially unbiased estimation of the ultimate torsional capacity. Moreover, the coefficient of variation (COV) is only 0.01, indicating very low scatter and a high level of consistency among the validation specimens.

The good agreement obtained for both the global torque–twist response and the ultimate torsional capacity confirm the ability of the adopted modeling approach to accurately reproduce the torsional behavior of both RC and SFRC beams with different reinforcement arrangements. Consequently, the validated FEM provides a reliable basis for the subsequent parametric investigations.

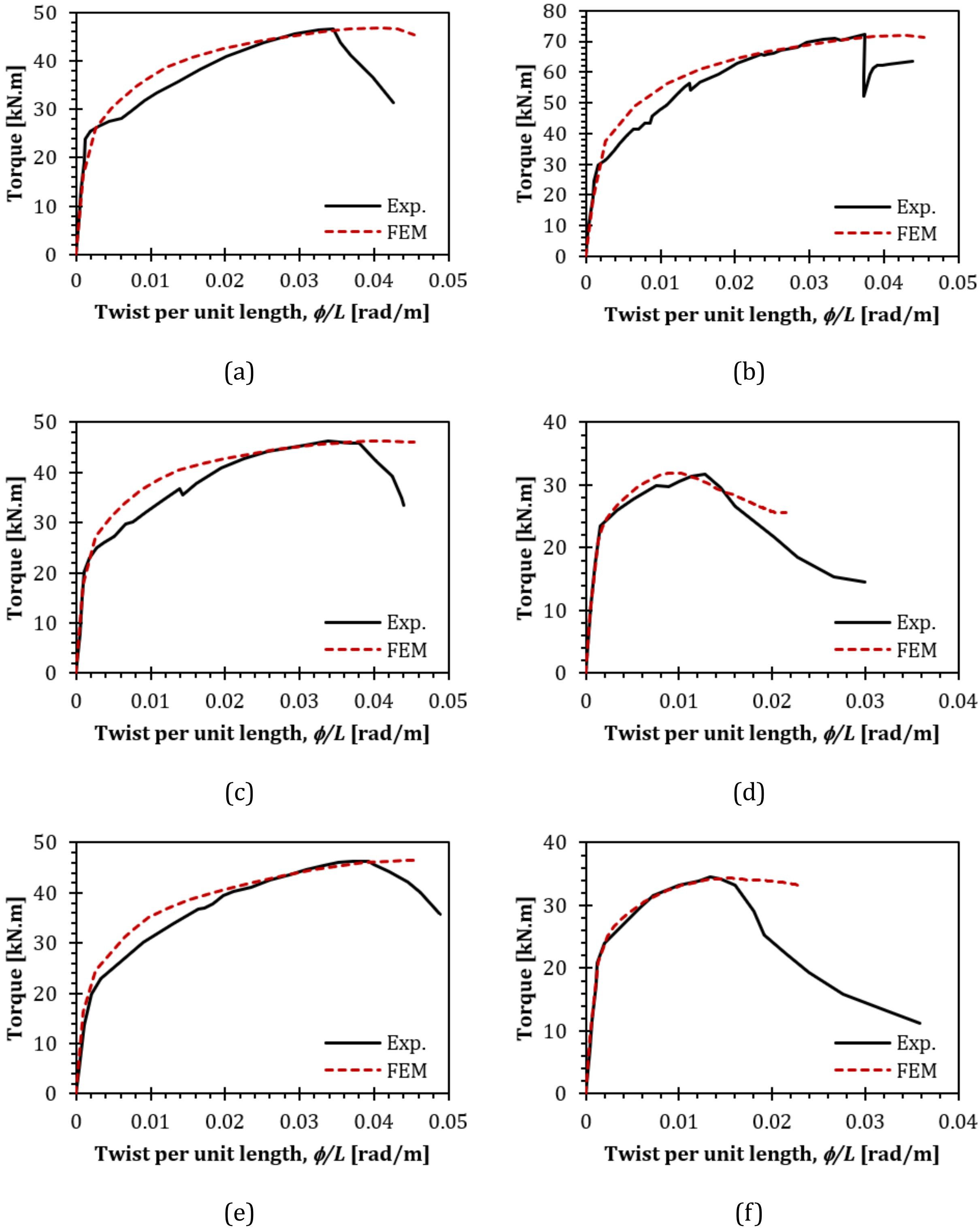

Figure 3. FEM vs experimental torque–twist responses of beams: (a) T1-PC-10/200; (b) T2-SFRC30-10/200; (c) T3-SFRC30-10/400; (d) T4-SFRC30-0; (e) T5-SFRC60-10/400; and (f) T6-SFRC60-0.

Table 3. Comparison of FEM predictions and experimental ultimate torsional capacities.

Specimen ID	$T_{u,test}$	$T_{u,FEM}$	$T_{u,test}/T_{u,FEM}$
T1-PC-10/200	46.7	46.9	1.00
T2-SFRC30-10/200	72.3	71.9	0.99
T3-SFRC30-10/400	46.3	46.2	1.00
T4-SFRC30-0	31.8	32.0	1.01
T5-SFRC60-10/400	46.3	46.4	1.00
T6-SFRC60-0	34.5	34.3	0.99
Mean			**1.00**
COV			**0.01**

5.1.2 Comparing the Test Results of Case Study Number II

To further evaluate the reliability of the developed FEM, additional validation was performed against the test results reported by **(Facconi et al., 2021a)**. The comparison between the predicted and measured torque–twist responses is presented in **Fig. 4** for three SFRC beams with different transverse reinforcement configurations.

Overall, the FEM demonstrates good agreement with the test results and successfully reproduces the key characteristics of the torsional response. The numerical predictions accurately capture the initial stiffness, cracking behavior, and ultimate torsional capacity of all tested specimens. In addition, the influence of transverse reinforcement on both strength and deformation capacity is consistently replicated by the numerical responses.

For specimen TB11-D50-L18-ST6/150 (**Fig. 4a**), the FEM closely replicates the experimental torque–twist response over all stages of loading. The predicted cracking torque, post-cracking stiffness, and ultimate torsional capacity show good agreement with the experimental results. Only minor differences in the residual torque are observed at larger twist levels, where the numerical model gives a slightly higher prediction than that measured experimentally.

Similarly, for specimen TB15-D50-L18-ST6/200 (**Fig. 4b**), the FEM captures both the ascending branch and the peak torque very well. The agreement remains satisfactory throughout the post-cracking region, although the numerical response exhibits a slightly smoother behavior. This difference is attributed to the smeared-crack formulation adopted in the CDPM, which tends to distribute damage over a finite region rather than representing localized crack development.

For specimen TB10-D50-L18 (**Fig. 4c**), which does not contain transverse reinforcement, the FEM provides a good prediction of both the ascending branch and the peak torsional capacity. The numerical model produces a post-peak softening response that is somewhat stronger than that observed experimentally. However, the overall response and failure load are predicted with reasonable accuracy.

Table 4 compares the experimentally measured ultimate torsional capacities with the corresponding FEM predictions for the specimens reported by **(Facconi et al., 2021a)**. The ratios of experimental-to-numerical ultimate torque were approximately 0.98 for all three specimens, with a mean value of 0.98 and a coefficient of variation close to zero. These results indicate that the FEM slightly overestimated the ultimate torsional resistance, but the predictions remained consistent and in good agreement with the experimental results.

The validation against the independent experimental program of **(Facconi et al., 2021a)** confirms the robustness of the developed modeling approach. The ability of the FEM to accurately reproduce the torsional behavior of SFRC beams from two separate experimental studies demonstrates that the adopted constitutive models and modeling assumptions provide a reliable representation of the mechanisms governing torsional resistance. The model is thus considered suitable for the parametric investigations presented in the subsequent sections.

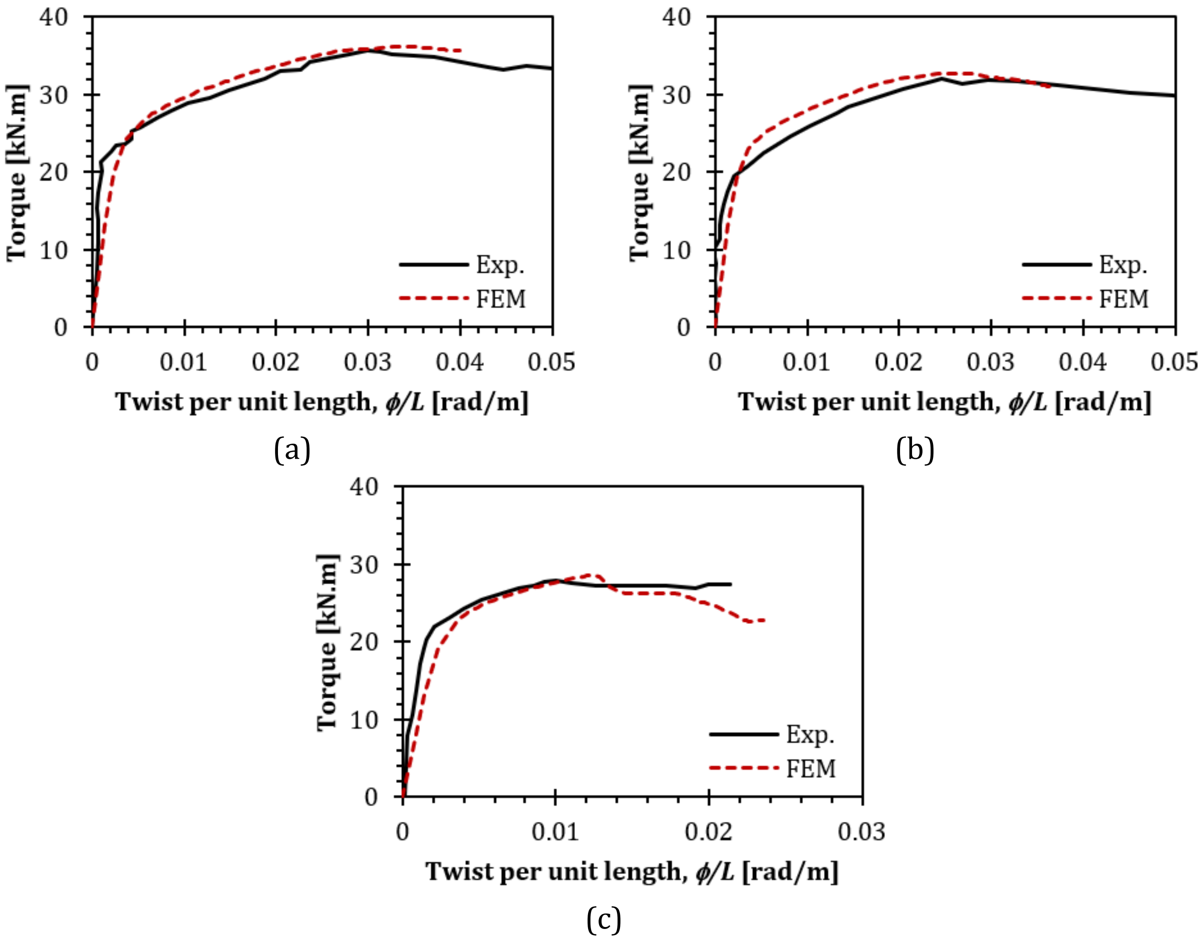

Figure 4. FEM vs experimental torque–twist responses of beams: (a) TB11-D50-L18-ST6/150; (b) TB15-D50-L18-ST6/200; (c) TB10-D50-L18.

Table 4. Comparison of FEM predictions and experimental ultimate torsional capacities for specimens reported by **(Facconi et al., 2021a)**.

Specimen ID	$T_{u,test}$	$T_{u,FEM}$	$T_{u,test}/T_{u,FEM}$
TB11-D50-L18-ST6/150	35.64	36.21	0.98
TB15-D50-L18-ST6/200	32.02	32.75	0.98
TB10-D50-L18	27.90	28.58	0.98
Mean			**0.98**
COV			**0.00**

5.2 Crack Patterns

Fig. 5 compares the crack patterns at peak load obtained from the FEM with those observed experimentally by **(Al-Damad et al., 2025)**. The contours shown in the FE results correspond to the distribution of plastic strains, which were used to identify the location and orientation of the principal torsional cracks.

In general, a fairly good agreement is obtained between the simulated crack patterns and those observed experimentally. For all specimens, the numerical analyses predict the formation of inclined helical cracks propagating along the beam length, which is a characteristic mode of torsional failure in reinforced concrete members. In addition, the predicted crack inclinations are in good agreement with the experimentally measured crack angles, indicating that the model captures the principal stress trajectories that develop under torsional loading.

For specimens T1-PC-10/200, T2-SFRC30-10/200, T3-SFRC30-10/400, and T5-SFRC60-10/400 (**Figs. 5a, 5c, 5e, and 5i**), the FEM predicts multiple distributed diagonal cracks similar to those observed experimentally. The predicted spacing and orientation of the crack bands match closely with the observed crack patterns, confirming that the model can capture the interaction between the concrete, steel fibers, and transverse reinforcement under torsional loading conditions.

This effect is especially evident when comparing specimens T2-SFRC30-10/200 and T3-SFRC30-10/400. In both the experimental and numerical results, a reduced transverse reinforcement ratio increases the crack spacing and reduces the number of diagonal cracks, while maintaining a similar crack inclination. The FEM can reflect this behavioral trend.

In the specimens without transverse reinforcement, namely T4-SFRC30-0 and T6-SFRC60-0 (**Figs. 5g and 5k**), the numerical analyses indicate more localized damage zones and fewer dominant crack bands, which are consistent with the experimental observations. In these specimens, torsional resistance is provided mainly by the steel fibers after cracking, leading to the development of wider and more concentrated cracks than in the stirrup-reinforced beams.

The close agreement between the predicted and observed crack patterns provides additional validation of the adopted constitutive models and modeling assumptions. In particular, the ability of the FEM to accurately reproduce both the global torque–twist response and the local cracking behavior demonstrate that the model can reliably capture the mechanisms governing torsional resistance in SFRC beams. Consequently, the developed FE model can be considered a reliable tool for investigating the torsional behavior of SFRC beams.

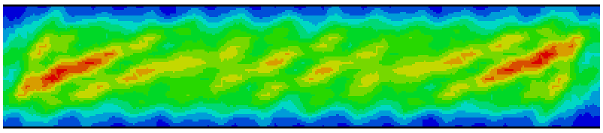

(a) Plastic strain at peak load of beam T1-PC-10/200

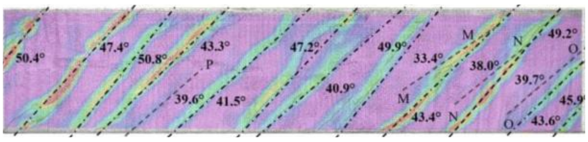

(b) Actual crack pattern of beam T1-PC-10/200 **(Al-Damad et al., 2025)**

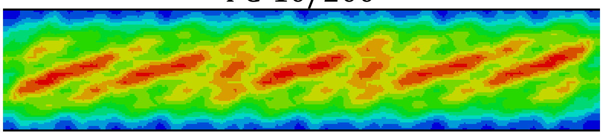

(c) Plastic strain at peak load of beam T2-SFRC30-10/200

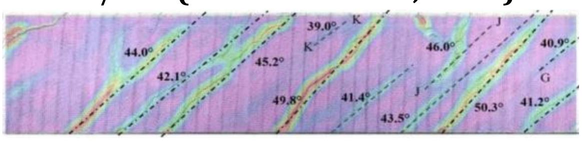

(d) Actual crack pattern of beam T2-SFRC30-10/200 **(Al-Damad et al., 2025)**

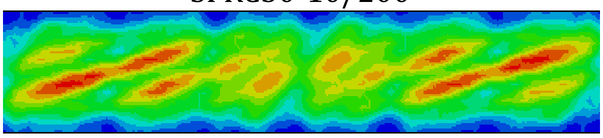

(e) Plastic strain at peak load of beam T3-SFRC30-10/400

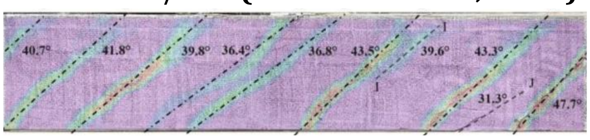

(f) Actual crack pattern of beam T3-SFRC30-10/400 **(Al-Damad et al., 2025)**

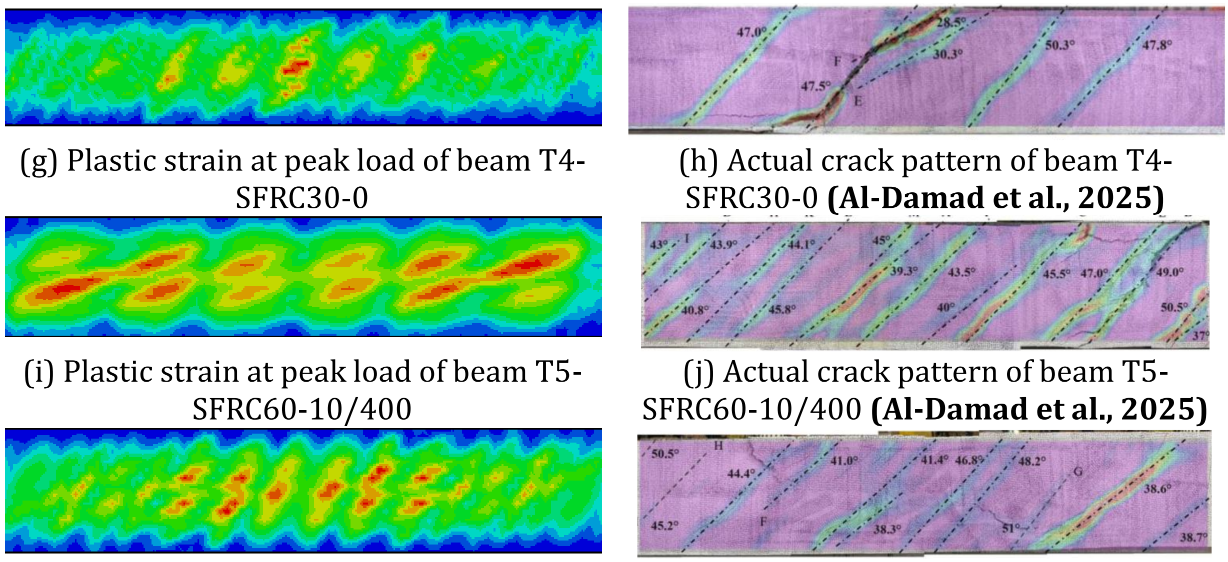

(g) Plastic strain at peak load of beam T4-SFRC30-0

(h) Actual crack pattern of beam T4-SFRC30-0 **(Al-Damad et al., 2025)**

(i) Plastic strain at peak load of beam T5-SFRC60-10/400

(j) Actual crack pattern of beam T5-SFRC60-10/400 **(Al-Damad et al., 2025)**

(k) Plastic strain at peak load of beam T6-SFRC60-0

(l) Actual crack pattern of beam T6-SFRC60-0 **(Al-Damad et al., 2025)**

Figure 5. Comparison of predicted tensile plastic strain contours and experimental crack patterns.

6. PARAMETRIC STUDY

Following validation against the test results, the developed FEM was used to investigate the influence of the key parameters governing the torsional behavior of SFRC beams. The parameters considered were the post-cracking softening behavior of SFRC, the transverse reinforcement ratio, and the concrete compressive strength. Particular emphasis was placed on the factors influencing the post-cracking response, ductility, and residual torsional resistance of SFRC members.

6.1 Effect of Post-Cracking Softening Behavior of SFRC

The post-cracking tensile response of SFRC is governed primarily by the fiber bridging action across cracks, which is commonly represented by a stress–COD relationship. To examine the influence of the SFRC softening behavior on the torsional response, parametric analyses were conducted by modifying the slope of the idealized stress–COD relationship derived from the dog-bone tensile tests.

Fig. 6 presents the stress–COD relationships adopted in the study. In addition to the idealized relationship obtained from the experimental data, three alternative constitutive models were considered. Case I is associated with a steeper softening response, indicating a lower residual tensile resistance, while Cases II and III are associated with progressively flatter softening responses, indicating greater fiber bridging capacity and enhanced crack resistance. In this investigation, the compressive strength of concrete and the transverse rebar ratio were kept constant to isolate the effect of the SFRC tensile softening behavior.

The effect of the adopted stress–COD relationships on the torsional response is shown in **Fig. 7** for specimen T4-SFRC30-0. The results show that the post-cracking performance is highly dependent on the tensile softening behavior of the SFRC. All constitutive relationships produce similar responses before cracking, but large differences are observed in the peak torsional capacity and in the post-cracking region.

In Case I, the tensile stress decreased quickly with increasing crack opening, which resulted in a large reduction in torsional resistance immediately after the peak load, leading to a brittle behavior with limited deformation capacity. By contrast, Cases II and III exhibited larger residual tensile stresses at larger crack opening displacements, allowing the fibers to continue transferring stresses across the torsional cracks. Therefore, both cases demonstrated better post-cracking behavior, higher residual torque capacities, and higher deformation capacities than the idealized constitutive relationship.

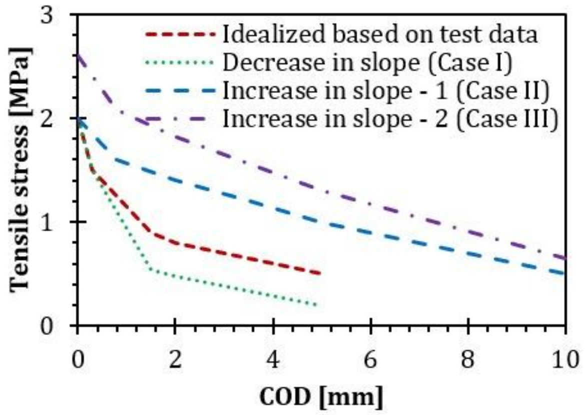

Figure 6. Stress–COD relationships adopted for the SFRC tensile softening study.

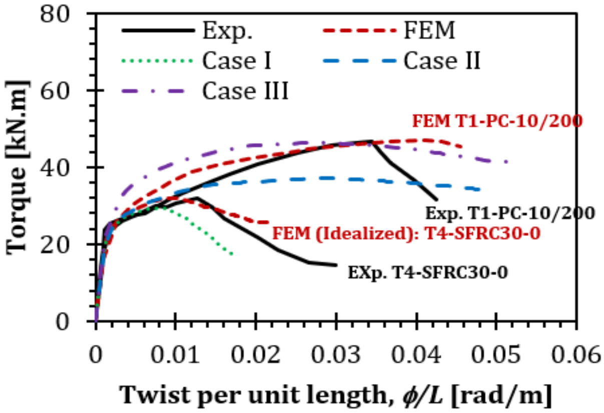

Figure 7. Effect of stress–COD relationship on torque–twist response of specimen T4-SFRC30-0.

It should be noted that Cases II and III were not intended to reproduce the experimental response of specimen T4-SFRC30-0. These cases were introduced as parametric tensile-softening scenarios to examine the effect of higher residual tensile resistance on the torsional response. Therefore, the improved torque–twist response obtained for Cases II and III reflects the expected influence of enhanced fiber-bridging capacity after cracking, rather than a direct validation against the experimental curve. The experimentally based stress–COD relationship was used as the validation case, whereas Cases II and III represent hypothetical improvements in the post-cracking tensile performance of SFRC.

For the investigated cases, Case III exhibited the highest residual torsional resistance and the most stable post-cracking response. The results show that the ductility of torsional members can be significantly improved and the deterioration of torsional resistance after cracking can be delayed by increasing the residual tensile capacity of SFRC. Besides, the predicted response of Case III is close to that of the conventionally reinforced beam T1-PC-10/200, which indicates that the lack of transverse rebar can be partially compensated by the improvement of fiber bridging performance.

These findings highlight the critical role of the SFRC tensile constitutive relationship in governing the post-cracking and post-peak behavior of torsional members. Although the influence on the cracking torsional capacity is relatively modest, the softening characteristics significantly affect the residual strength, deformation capacity, and overall ductility of SFRC beams subjected to torsion. Consequently, accurate characterization of the post-cracking tensile behavior of SFRC is essential for reliable numerical modeling and design of torsion-critical members.

6.2 Concrete Compressive Strength Influence

To investigate the influence of compressive strength of concrete on the torsional behavior of SFRC members, a parametric investigation was conducted by changing the compressive strength of concrete while keeping the SFRC tensile constitutive relationship and the transverse reinforcement ratio unchanged. Four concrete compressive strengths were considered: 35 MPa, 60 MPa, 80 MPa, and 100 MPa. These values cover a wide range of practical concrete strengths and allow the contribution of the concrete matrix to the torsional response to be evaluated separately from fiber and reinforcement effects. The 80 MPa and 100 MPa cases were treated as HSC cases using the same CDPM framework described in Section 4.2, with strength-dependent elastic, compressive, and tensile material properties.

The predicted torque–twist responses of beams with several concrete compressive strength is shown in **Fig. 8**. The results show that the compressive strength of concrete has a strong influence on the cracking torque, ultimate torsional capacity, and post-cracking behavior of the beams. The increase in concrete compressive strength leads to a stiffer response and higher torsional resistance for both specimens along the loading history.

The effect of concrete strength is more pronounced after cracking. The torque–twist response of the 35 MPa concrete shows a lower post-cracking stiffness and a reduced torsional capacity. Higher torque capacities are achieved with increasing compressive strength from 35 to 60, 80, and 100 MPa. The increase is associated with an improvement of the post-cracking behavior, which suggests that a stronger concrete provides more effective compression struts in the torsion-resisting mechanism.

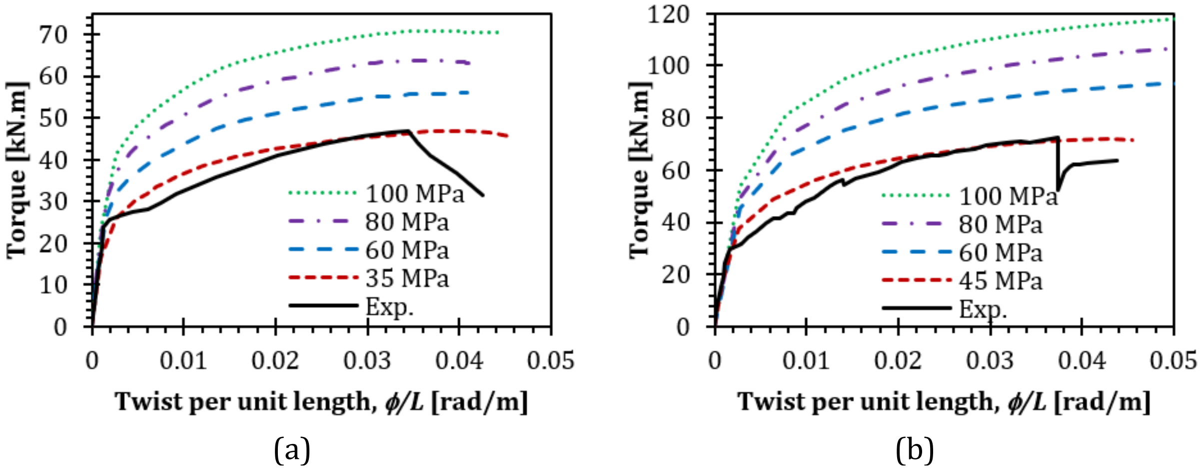

Figure 8. Torque-twist for different concrete compressive strengths for the specimens: (a) T1-PC-10/200; (b) T2-SFRC30-10/200.

For the plain concrete specimen T1-PC-10/200 (**Fig. 8a**), the increase of concrete compressive strength leads to a significant increase of both peak torque and deformation capacity. A similar behavior can be observed for the SFRC specimen T2-SFRC30-10/200 (**Fig. 8b**) where the beneficial effect of increasing the concrete strength is enhanced by the residual tensile resistance provided by the steel fibers. Thus, the SFRC beam has higher torque levels over a wider range of twist values compared to the conventional reinforced concrete beam.

The increase in torsional capacity was not in proportion to the increase in concrete compressive strength. Significant gains were observed when the compressive strength increased from 35 to 60 and 80 MPa but the incremental benefit was reduced at higher strengths. This behavior indicates that, beyond a certain level, the torsional response is increasingly governed by the tensile properties of the cracked concrete, the fiber bridging action and the contribution of the reinforcement, rather than only by the compressive strength of the concrete matrix.

In general, the findings reveal that increasing concrete compressive strength improves torsional behavior and ductility of SFRC members. However, the data also demonstrate that the potential benefits to torsional performance gained from improvements in compressive strength are not realized for SFRC beams unless supplemented with suitable post-cracking tensile resistance resulting from fiber contribution and appropriate transverse reinforcement. These findings highlight the significance of assessing not just compressive but also tensile material characteristics when designing SFRC members for torsion.

6.3 Transverse Reinforcement Ratio Effect

The stirrups ratio is one of the primary parameters governing the torsional resistance of RC and SFRC members. To investigate its influence on the torsional behavior of SFRC members, a parametric analysis was performed by varying the stirrups ratio through two independent parameters: stirrup bar diameter and stirrup spacing. Stirrup diameters of 8 mm, 10 mm, and 12 mm were considered, while stirrup spacing values were taken as 100 mm, 200 mm, 300 mm, and 400 mm. For comparison purposes, additional analyses were performed for beams without stirrups. Throughout the study, the concrete compressive strength and the SFRC tensile constitutive relationship were maintained constant so that the influence of the stirrup ratio could be isolated.

6.3.1 Effect of Stirrup Bar Diameter

The **Fig. 9** compares the torque–twist responses obtained for different stirrup bar diameters. In general, increasing the stirrup diameter raised both the torsional capacity and the post-cracking stiffness of the members. The effect of stirrup diameter was relatively limited before cracking but became increasingly significant after the formation of torsional cracks, where the transverse reinforcement contributes directly to the space-truss mechanism.

For all specimens, increasing the stirrup diameter from 8 mm to 12 mm produced only a modest increase in peak torque. The larger-diameter stirrups, however, gave a more stable post-cracking response and sustained higher torque levels at larger twist values. The effect was most noticeable for specimen T2-SFRC30-10/200 (**Fig. 9b**), where increasing the stirrup diameter results in a clear enhancement in both deformation capacity and torsional strength.

In contrast, the effect of stirrup diameter becomes less pronounced for specimens T3-SFRC30-10/400 and T5-SFRC60-10/400 (**Figs. 9c** and **9d**). For these beams, the torque–

twist responses corresponding to different stirrup diameters remain relatively close, indicating that the contribution of additional stirrup area is partially compensated by the residual tensile resistance provided by the steel fibers. This observation suggests that fibers can reduce the sensitivity of the torsional response to changes in stirrup reinforcement.

Overall, the findings indicate that increasing the stirrup bar diameter enhances the torsional resistance of SFRC beams, although the magnitude of the improvement is relatively modest compared with other parameters investigated in this study.

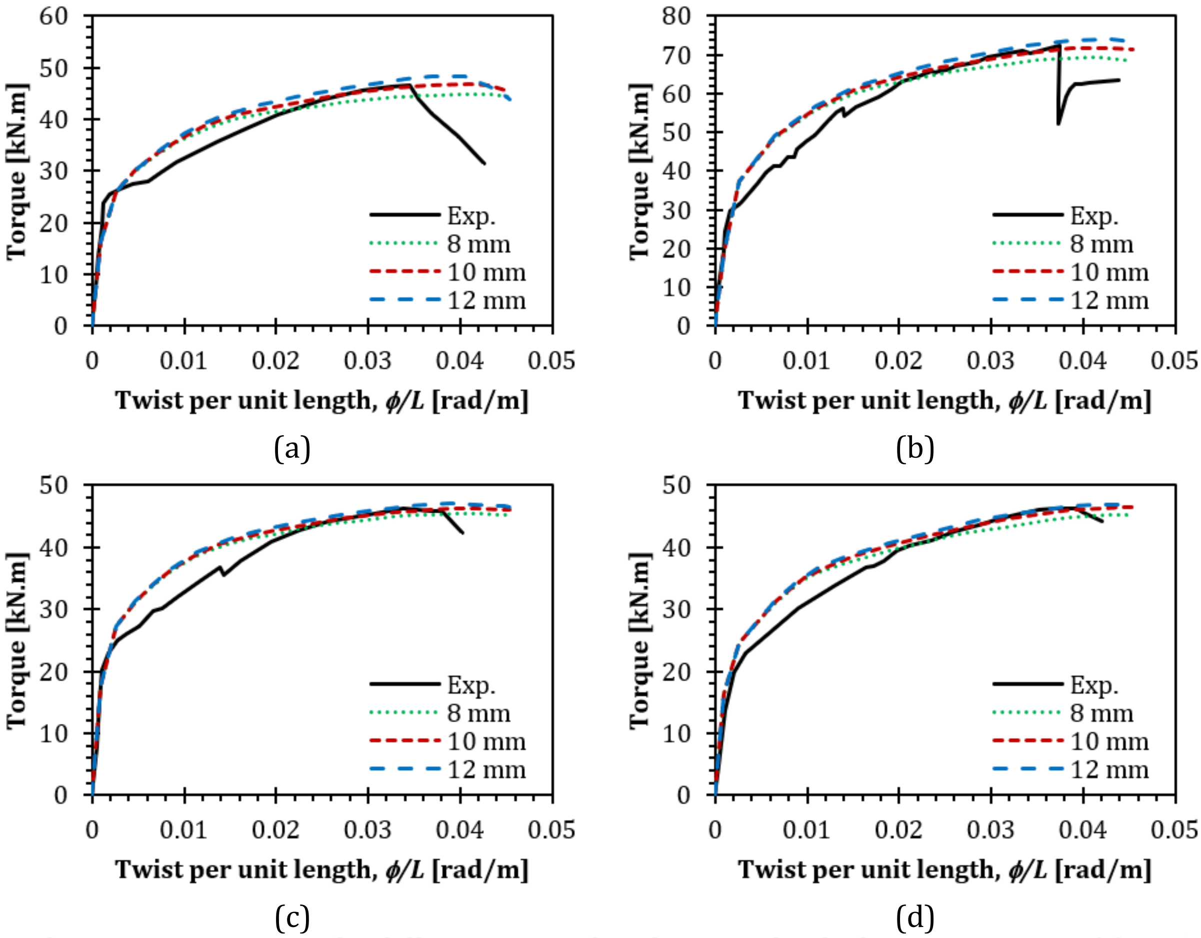

Figure 9. Torque-twist for different stirrup bar diameter for the beam specimens: (a) T1-PC-10/200; (b) T2-SFRC30-10/200; (c) T3-SFRC30-10/400; (d) T5-SFRC60-10/400.

6.3.2 Effect of Stirrup Spacing

The **Fig. 10** presents the torque–twist responses obtained for different stirrup spacings. Compared with the variation in stirrup diameter, changing the stirrup spacing had a substantially greater influence on the torsional behavior of the beams.

For specimen T1-PC-10/200 (**Fig. 10a**), decreasing the stirrup spacing results in significant improvements in both the peak torque and post-cracking response. The specimen with a spacing of 100 mm had the highest torsional capacity and deformation capacity, while the response progressively worsens as the spacing increases. The 400 mm spacing specimen shows a notably lower torsional resistance and brittle behavior.

A similar trend is observed for the SFRC specimens shown in **Figs. 10b** and **10c**. It was also observed that the minimum stirrup spacing would increase peak torsional capacity and residual torsional resistance after cracking. The torsional behavior of the beams containing transverse reinforcement (i.e., stirrups spaced at closer intervals) is particularly improved because this spacing encourages the formation of a more beneficial truss mechanism and better crack control.

The comparison between the stirrup-reinforced and unreinforced beams amplifies the importance of transverse reinforcement. Specimens without stirrups meet considerable post-cracking tensile resistance due to the steel fibers yet demonstrate much lower torsional capacities and more rapid post-cracking softening than their stirrup-reinforced counterparts. This behavior demonstrates that fiber alone cannot fully replace the role of transverse reinforcement in resisting torsion.

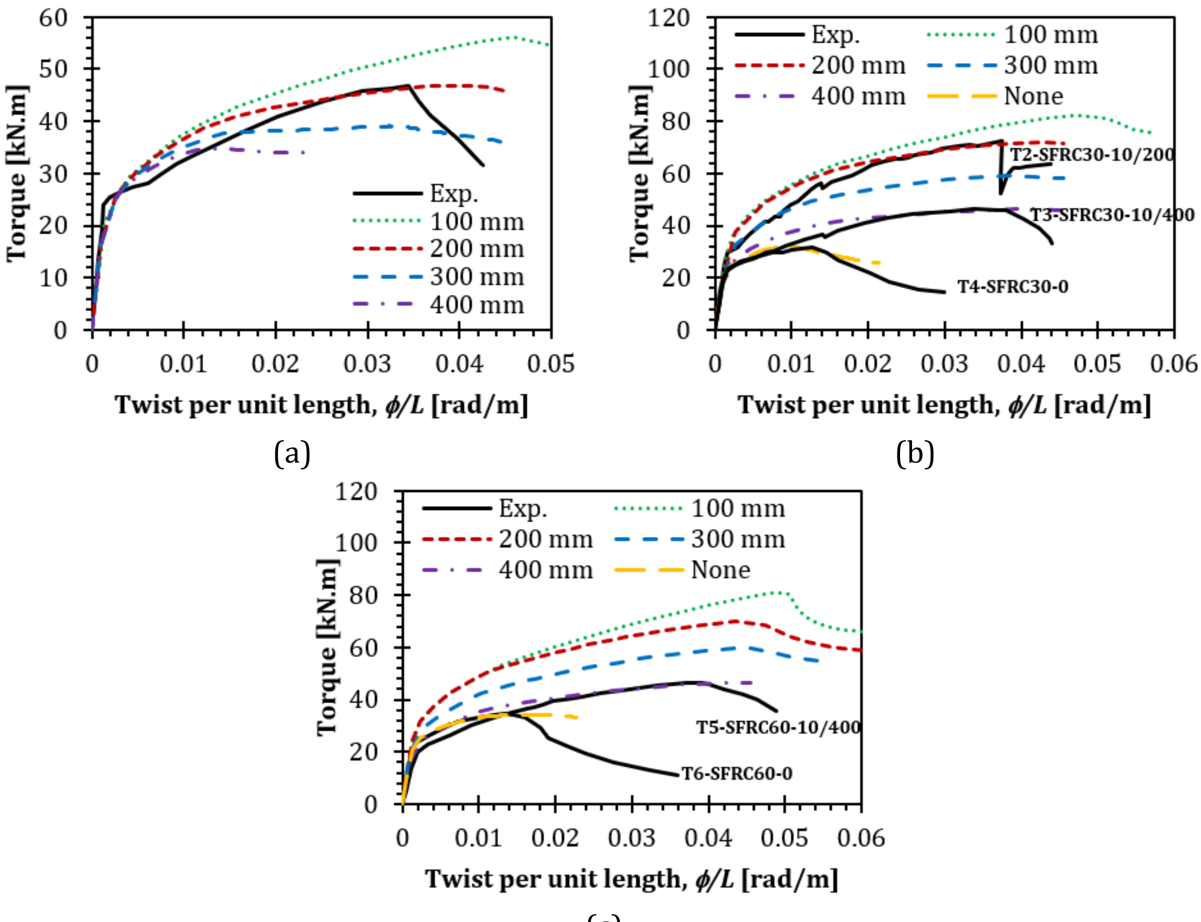

Figure 10. Torque-twist for different stirrup spacing for the beam specimens: (a) T1-PC-10/200; (b) T2-SFRC30-10/200, T3-SFRC30-10/400 and T4-SFRC30-0; (c) T5-SFRC60-10/400 and T6-SFRC60-0.

The results also show that reducing stirrup spacing is more effective than increasing stirrup diameter for enhancing torsional performance. While increasing the bar diameter only marginally increases the transverse reinforcement ratio, reducing the spacing increases the number of stirrups intersecting the torsional cracks and improves the efficiency of the torsion-resisting mechanism. Consequently, stirrup spacing has a much greater influence on torsional strength, post-cracking stiffness, and deformation capacity than stirrup diameter.

Overall, the parametric study confirms that the transverse reinforcement ratio remains a key parameter governing the behavior of SFRC beams subjected to torsion. Although steel fibers contribute significantly to the post-cracking response, adequate transverse reinforcement is still required to achieve high torsional strength, stable post-peak behavior, and improved deformation capacity.

6.4 Discussion of Parametric Study Results

The numerical results demonstrate that the torsional behavior of SFRC beams is governed by the interaction between the tensile properties of the SFRC, the transverse rebar ratio, and the concrete compressive strength. Although all three parameters affect the response, their effects vary considerably over the loading history.

The angle of twist is an important response parameter because it reflects the deformation demand associated with torsional loading. Beams that maintained higher torque at larger twist values exhibited a more stable post-cracking response and greater deformation capacity. The parametric results showed that flatter SFRC tensile softening curves improved residual torque at larger twists, while closer stirrup spacing delayed the degradation of torsional resistance by improving crack control. In contrast, beams without transverse reinforcement showed more rapid strength degradation after cracking, indicating that fiber bridging alone was less effective in sustaining torsional resistance at higher twist levels.

The post-cracking tensile behavior of SFRC had a dominant influence on residual torsional resistance and deformation capacity. This trend is consistent with previous studies showing that fiber bridging across cracks enhances post-cracking stress transfer, crack control, and torsional resistance in SFRC members **(Amin and Bentz, 2018; Facconi et al., 2021a; Al-Damad et al., 2025)**.

The cracking and ultimate torsional capacities were found to depend on the concrete compressive strength. As the compressive strength increased, the torsional resistance over the loading history was greater due to the better capacity of the concrete compression struts within the torsional resistance mechanism. The increase in torsional capacity, however, was not proportional to the compressive strength, indicating a combined effect of both compressive and tensile material characteristics governing the behavior of SFRC torsional members. Similar observations have been reported in analytical and experimental studies on torsion, where the concrete compression field and post-cracking tensile mechanisms jointly govern the torsional response **(Rao and Seshu, 2005; Ju et al., 2015; Oettel, 2023)**.

The transverse reinforcement ratio was also an important parameter affecting torsional behavior. Post-cracking stiffness, peak torsional capacity, and residual torsional resistance are enhanced with the increasing amount of transverse reinforcement. Of the parameters, decreasing the stirrup spacing yielded a much larger increase in torsional performance than increasing the bar diameter. This is ascribed to the higher number of stirrups intersecting the torsional crack surfaces, which increases the effectiveness of the torsional truss mechanism and allows better control over cracks. The stronger influence of stirrup spacing compared with bar diameter is consistent with the torsional truss mechanism, where a larger number of stirrups intersecting diagonal torsional cracks improves crack distribution and post-cracking resistance **(Macgregor and Wight, 2005; Amin and Bentz, 2018; Al-Damad et al., 2025)**.

The analyses also showed that the contributions of steel fibers and transverse reinforcement to torsional resistance are complementary. The fibers mainly increase the residual tensile resistance after cracking and improve the post-cracking behavior, while the stirrups directly contribute to resisting torsion via a truss mechanism. Despite the major enhancement of torsional behavior observed for beam specimens without stirrups when fibers are added, the results suggest that such fibers cannot yet be considered as a complete alternative to conventional transverse reinforcement. As a result, the best possible torsional performance is achieved when both mechanisms are mobilized simultaneously. This agrees with the experimental findings of **(Facconi et al., 2021a; Al-Damad et al., 2025)**, where the combined use of fibers and conventional transverse reinforcement improved strength, crack distribution, and deformation capacity more effectively than fibers alone.

In general, the numerical results indicate that it is essential to accurately account for the post-cracking tensile behavior of SFRC in torsional members. The established and validated FEM generated valuable information on the role of each, and the combined contributions of fibers, concrete strength, and stirrups in optimizing the torsional resistance of SFRC specimens.

7. CONCLUSIONS

A three-dimensional nonlinear finite element model was developed in ABAQUS to investigate the torsional behavior of steel fiber reinforced concrete (SFRC) beams subjected to pure torsion. The model was validated against experimental results available in the literature in terms of torque–twist response, ultimate torsional capacity, and crack patterns. A parametric study was then conducted to examine the effects of SFRC tensile softening behavior, concrete compressive strength, and transverse reinforcement ratio. The main conclusions are as follows:

- The developed FE model reproduced the experimental torque–twist response and ultimate torsional capacity with good accuracy. The numerical-to-experimental ultimate torsional capacity ratio ranged from 0.99 to 1.01, with a mean value of 1.00 and a coefficient of variation of 0.01.
- The predicted tensile plastic strain contours showed inclined helical damage bands consistent with the torsional crack patterns experimentally observed. This indicates that the model can represent the dominant local damage mechanisms under pure torsion.
- SFRC post-cracking tensile behavior largely influenced residual torsional resistance, response and deformation capacity. The stability of the post-cracking response was enhanced by higher residual tensile stresses in the stress–COD relationship.
- The tensile softening behavior of SFRC is substantially variable in nature and hence should be considered in numerical modeling since the residual tension resistance depends on fiber distribution, fiber orientation as well as number of fibers crossing crack plane.
- Higher compressive strength of concrete enhanced both cracking torque and ultimate torsional capacity. Yet the increase in torsional capacity was not proportional to the increase of compressive strength, which implied that both compressive and post-cracking tensile mechanisms control response.
- Transverse reinforcement still remained necessary for torsional resistance. Torsional cracks were significantly reduced with closer stirrup spacing, which comprised a stronger factor than increasing the diameter of already very large bar sizes; such improved crack control is due to more intersecting stirrups for shorter torsion spans.
- Steel fibers and transverse reinforcement provided complementary contributions to torsional resistance. Steel fibers improved the post-cracking tensile resistance due to

crack-bridging action, and stirrups played a direct role in the torsion-resisting mechanism. Hence steel fibers improved the behavior of beams without stirrups and did not fully replace traditional transverse reinforcement.

Credit Authorship Contribution Statement

Hayder A. Al-Baghdadi: Writing – original draft, Project administration, Formal analysis. Iman Munadhil Abbas Al-Damad: Writing – original draft, Conceptualization, Project administration, Formal analysis. Ehab G. Al-Hasany: Writing – review & editing, Validation, Software. Mustafa Qasim Dows: Writing – review & editing.

Declaration of Competing Interest

The authors declare that they have no known competing financial interests or personal relationships that could have appeared to influence the work reported in this paper.

REFERENCES

ACI 318, 2019. Building code requirements for reinforced concrete and commentary (ACI 318). Detroit: American Concrete Institute.

Al-Damad, I.M.A., and Foster, S.J., 2022. Behavior of postcracked steel fiber-reinforced concrete in fatigue and development of a damage prediction model. *Structural Concrete*, *23*(3), pp. 1593-1610. https://doi.org/10.1002/suco.202100497

Al-Damad, I.M.A., Parvez, A., Kumar, L.M. and Foster, S.J., 2025. Experimental study on steel fibers reinforced concrete beams subjected to pure torsion and models assessment. *Structural Concrete*, *26*(5), pp. 6180-6202. https://doi.org/10.1002/suco.70168

Amin, A., 2015. Post cracking behaviour of steel fibre reinforced concrete: from material to structure, PhD Thesis, School of Civil and Environmental Engineering, University of New South Wales, Australia

Amin, A., and Bentz, E.C., 2018. Strength of steel fiber reinforced concrete beams in pure torsion. *Structural concrete*, 19(3), pp. 684-694. https//:doi.org/10.1002/suco.201700183

AS3600, 2018. Concrete structures. Australian Standard, Standards Association of Australia.

Chalioris, C.E., and Karayannis, C.G., 2009. Effectiveness of the use of steel fibres on the torsional behaviour of flanged concrete beams. *Cement and Concrete Composites*, *31*(5), pp.331-341. https://doi.org/10.1016/j.cemconcomp.2009.02.007

Chen, W.F., Han, D.J. and Han, D.J., 2007. *Plasticity for Structural Engineers*. J. Ross publishing.

Dassault Systèmes, 2019. *Abaqus 2019*. Providence, RI, USA: SIMULIA, Dassault Systèmes

Deutscher Ausschuss für Stahlbeton (DAfStb), 2015. Commentary on the DAfStb Guideline "Steel Fibre Reinforced Concrete." DAfStb-Heft 614. Berlin: Beuth Verlag.

El-Niema, E.I., 1993. Fiber reinforced concrete beams under torsion. *Structural Journal*, *90*(5), pp. 489-495.

Faccin, E., Facconi, L., Minelli, F., and Plizzari, G., 2021, September. Predicting the residual flexural strength of concrete reinforced with hooked-end steel fibers: new empirical equations. In *RILEM-fib International Symposium on Fibre Reinforced Concrete*, pp. 456-468.

Facconi, L., Amin, A., Minelli, F., and Plizzari, G., 2021a. A unified approach for determining the strength of FRC members subjected to torsion—Part I: Experimental investigation. *Structural Concrete*, *22*(6), pp. 3763-3779. https://doi.org/10.1002/suco.202100161

Facconi, L., Amin, A., Minelli, F., and Plizzari, G., 2021b. A unified approach for determining the strength of FRC beams subjected to torsion–Part II: Analytical modeling. *Structural Concrete*, *22*(6), pp. 3780-3797. https://doi.org/10.1002/suco.202100162

Facconi, L., Amin, A., Minelli, F., and Plizzari, G., 2025. Recent developments in torsion design of SFRC elements. *Special Publication*, *365*, pp. 17-34.

Fédération internationale du béton (fib), 2013. *fib Model Code for Concrete Structures 2010*. Lausanne: Fédération internationale du béton (fib). Available at: Wiley Online Library (Accessed: 10 July 2026). https://doi.org/10.1002/9783433604090.

Foster, S.J., and Voo, Y.L., 2004. Finite element modelling of fibre reinforced concrete structures. *Developments in Mechanics of Structures and Materials, 18th Australasian Conference on the Mechanics of Structures and Materials. Perth, Western Australia*. Eds A. Deeks and H. Hoa, Taylor and Francis, London, pp. 781-787.

Foster, S.J., Voo, Y.L., and Chong, K.T., 2006. FE analysis of steel fiber reinforced concrete beams failing in shear: variable engagement model. *Special Publication*, *237*, pp. 55-70.

Hordijk, D.A., 1992. Tensile and tensile fatigue behaviour of concrete; experiments, modelling and analyses. *Heron*, *37*(1).

Ju, H., Kim, K.S., Lee, D.H., Hwang, J.H., Choi, S.H., and Oh, Y.H., 2015. Torsional responses of steel fiber-reinforced concrete members. *Composite Structures*, *129*, pp. 143-156. https://doi.org/10.1016/j.compstruct.2015.04.003

Lee, J., and Fenves, G.L., 1998. Plastic-damage model for cyclic loading of concrete structures. *Journal of Engineering Mechanics*, *124*(8), pp. 892-900. https://doi.org/10.1061/(ASCE)0733-9399(1998)124:8(892)

Lee, D.H., Hwang, J.H., Ju, H., Kim, K.S., and Kuchma, D.A., 2012. Nonlinear finite element analysis of steel fiber-reinforced concrete members using direct tension force transfer model. *Finite Elements in Analysis and Design*, *50*, pp. 266-286. https://doi.org/10.1016/j.finel.2011.10.004

Lim, T.Y., Paramasivam, P., and Lee, S.L., 1987. Analytical model for tensile behavior of steel-fiber concrete. *Materials Journal*, *84*(4), pp. 286-298.

Lövgren, I., 2005. Fibre-reinforced concrete for industrial construction–a fracture mechanics approach to material testing and structural analysis. PhD Thesis, Department of Civil and Environmental Engineering, Chalmers University of Technology, Sweden.

Lubliner, J., Oliver, J., Oller, S., and Onate, E., 1989. A plastic-damage model for concrete. *International Journal of Solids and Structures*, *25*(3), pp. 299-326. https://doi.org/10.1016/0020-7683(89)90050-4

Macgregor, J.G., and Wight, J.K., 2005. *Reinforced Concrete: Mechanics And Design*. Hoboken, NJ: Prentice-Hall.

Mansur, M.A., Nagataki, S., Lee, S.H., and Oosumimoto, Y., 1989. Torsional response of reinforced fibrous concrete beams. *Structural Journal*, *86*(1), pp. 36-44.

Minelli, F., 2005. Plain and fiber reinforced concrete beams under shear loading: Structural behavior and design aspects. PhD Thesis, Department of Civil Engineering, University of Brescia, Italy.

Minelli, F., and Vecchio, F.J., 2006. Compression field modeling of fiber-reinforced concrete members under shear loading. *ACI Structural Journal*, *103*(2), P. 244.

Oettel, V., 2023. Steel fiber reinforced RC beams in pure torsion—Load-bearing behavior and modified space truss model. *Structural Concrete*, *24*(1), pp. 1348-1363. https://doi.org/10.1002/suco.202200031

Okay, F., and Engin, S., 2012. Torsional behavior of steel fiber reinforced concrete beams. *Construction and Building Materials*, *28*(1), pp. 269-275. https://doi.org/10.1016/j.conbuildmat.2011.08.062

Pfyl, T., 2003. Tragverhalten von stahlfaserbeton. PhD Thesis, Swiss Federal Institute of Technology, Switzerland. (in German).

Rakaa, R.K., and Abbas, R.M., 2024. Mechanical properties of lightweight EPS self-compacting concrete reinforced with steel fibers. *Journal of Engineering*, 30(6), pp. 125-140. https://doi.org/10.31026/j.eng.2024.06.08.

Rao, T.G., and Seshu, D.R., 2005. Analytical model for the torsional response of steel fiber reinforced concrete members under pure torsion. *Cement and Concrete Composites*, *27*(4), pp. 493-501. https://doi.org/10.1016/j.cemconcomp.2004.03.006

Reuter, U., Sultan, A., and Reischl, D.S., 2018. A comparative study of machine learning approaches for modeling concrete failure surfaces. *Advances in Engineering Software*, *116*, pp. 67-79. https://doi.org/10.1016/j.advengsoft.2017.11.006

Saenz, L.P., 1964. Discussion of equation for the stress-strain curve of concrete. *ACI Journal*, *61*, pp. 1227-1239.

التحليل اللاخطي بالعناصر المحددة للعتبات الخرسانية المسلحة بالألياف الفولاذية والخاضعة للالتواء الخالص

حيدر عامر البغدادي[1]، إيمان مناضل عباس الداماد[1]، *، إيهاب غازي الحسني[2]، مصطفى قاسم دوس[3]

[1] قسم الهندسة المدنية، كلية الهندسة، جامعة بغداد، بغداد، العراق

[2] المشاريع الممولة من البنك الدولي، وزارة التربية، بغداد، العراق

[3] قسم الهندسة الميكانيكية، كلية الهندسة، جامعة بغداد، بغداد، العراق

الخلاصة

تعد الألياف الفولاذية فعالة في تعزيز مقاومة الشد بعد التشقق في الخرسانة، وذلك من خلال نقل الإجهادات عبر الشقوق. وعلى الرغم من أن عدداً من المدونات والمواصفات التصميمية الدولية تسمح بأخذ مساهمة الألياف بنظر الاعتبار في الانحناء والقص، إلا أن الإرشادات التصميمية الصريحة للعناصر الخرسانية المسلحة بالألياف الفولاذية والخاضعة للالتواء ما زالت محدودة. لذلك، لا يزال تصميم الالتواء يعتمد بصورة رئيسية على التسليح العرضي التقليدي، في حين تُهمل مساهمة الألياف أو لا تُستثمر بالشكل الكافي. تقدم هذه الدراسة تحليلاً عددياً لاخطياً ثلاثي الأبعاد باستخدام طريقة العناصر المحددة للعناصر الخرسانية المسلحة بالألياف الفولاذية والخاضعة للالتواء الخالص باستخدام برنامج ABAQUS. تم تطوير النموذج العددي بالاعتماد على نموذج اللدونة المتضررة للخرسانة، وتم التحقق منه من خلال مقارنته مع نتائج تجارب مستقلة متوفرة في الأدبيات. أظهرت المقارنة توافقاً جيداً بين التنبؤات العددية والملاحظات التجريبية من حيث استجابة العزم الالتوائي–الدوران، والمقاومة الالتوائية القصوى، وأنماط التشقق. وبعد التحقق من النموذج، أُجريت دراسة للمتغيرات لبحث تأثير سلوك التليين في الشد بعد التشقق للخرسانة المسلحة بالألياف الفولاذية، ومقاومة الانضغاط للخرسانة، ونسبة الأساور على الاستجابة الالتوائية. بينت النتائج أن أداء الشد بعد التشقق للخرسانة المسلحة بالألياف الفولاذية يؤثر بصورة واضحة في المقاومة الالتوائية المتبقية، والاستجابة بعد التشقق، وقابلية التشوه. كما أن التغيرات في سلوك التليين في الشد، الناتجة عن الطبيعة العشوائية لتوزيع الألياف واتجاهها، أثرت بصورة ملحوظة في الاستجابة الالتوائية المتوقعة. وأدت زيادة مقاومة الانضغاط للخرسانة إلى تحسين كل من عزم التشقق والمقاومة الالتوائية القصوى. كما كان تقليل تباعد الأساور أكثر تأثيراً من زيادة قطر سيخ الأسورة في تحسين الأداء الالتوائي. وتؤكد النتائج أن الألياف الفولاذية والتسليح العرضي يقدمان مساهمتين متكاملتين في مقاومة الالتواء.

الكلمات المفتاحية: التحليل بالعناصر المحددة، استجابة العزم الالتوائي–الدوران، الخرسانة المسلحة بالألياف الفولاذية، الالتواء النقي، سلوك ما بعد التشقق.